Manganese Clusters

International Edition: DOI: 10.1002/anie.201800079
German Edition: DOI: 10.1002/ange.201800079

A Manganese Nanosheet: New Cluster Topology and Catalysis

*Uttam Chakraborty, Efrain Reyes-Rodriguez, Serhiy Demeshko, Franc Meyer, and Axel Jacobi von Wangelin**

Abstract: *While the coordination chemistry of monometallic complexes and the surface characteristics of larger metal particles are well understood, preparations of molecular metallic nanoclusters remain a great challenge. Discrete planar metal clusters constitute nanoscale snapshots of cluster growth but are especially rare owing to the strong preference for three-dimensional structures and rapid aggregation or decomposition. A simple ligand-exchange procedure has led to the formation of a novel heteroleptic Mn_6 nanocluster that crystallized in an unprecedented flat-chair topology and exhibited unique magnetic and catalytic properties. Magnetic susceptibility studies documented strong electronic communication between the manganese ions. Reductive activation of the molecular Mn_6 cluster enabled catalytic hydrogenations of alkenes, alkynes, and imines.*

Two-dimensional materials have gained a strong foothold in the rapidly developing field of nanoscience. Carbon nanosheets and monolayers of metals and other elements show profoundly different physical properties from the bulk systems.[1] Unlike graphene, transition-metal nanosheets are very challenging to prepare owing to the lack of convenient metal precursors, the preference for three-dimensional geometries, and the generally high reactivity of metal monolayers.[2] Consequently, only very few examples of small transition-metal nanosheets with planar or raft-like arrangements of the metal atoms have been reported. The vast majority of transition-metal clusters contain six or more metal atoms in three-dimensional cluster geometries.[3,4] From a conceptual viewpoint, 3D metal nanoclusters are models of the bulk material. Small 2D metal nanoclusters can be viewed as intermediate stages of the growth of soluble metals or metal ions towards metallic monolayers (Figure 1).[5] Flat

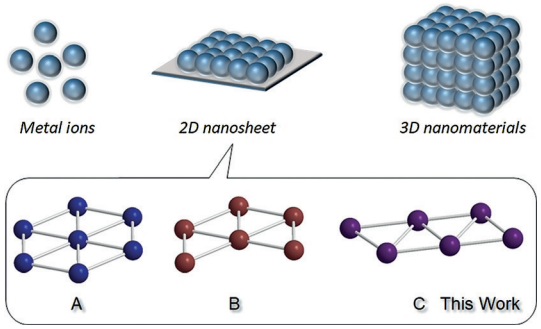

Figure 1. Growth of 2D and 3D transition-metal architectures.

metal clusters exhibit unique magnetic properties and distinct catalytic activities owing to the electronic, magnetic, and steric communication between the neighboring metals in the plane. Polynuclear metal carbonyl species are by far the most studied class of 2D and 3D clusters; they exhibit strong coordination of the CO ligands to the metals, are coordinatively saturated, and thus provide not the best models for metal clusters and surfaces under other, CO-free conditions.[4] An example of a planar, CO-free cluster is the oligohydride Rh_7 wheel (type **A**, Figure 1), which contains a planar Rh core that mimics a M(111) monolayer.[3] Recently, Ohki and coworkers and our group have shown that the reaction of easily available transition-metal amide precursor complexes $M\{N(SiMe_3)_2\}_2$ (M = Co, Fe) with commercial hydride sources (diisobutylaluminium hydride, Dibal-H; pinacolborane, HBpin) is a convenient strategy to access new topologies of low-valent transition-metal nanoclusters in high yields. Planar Co_4, Co_7, Fe_4, Fe_6, and Fe_7 clusters have been isolated and characterized. Among the larger metal clusters with six or more metal atoms, the type **A** topology has been realized with Fe and Co, and the truncated wheel of type **B** with Fe.[3] Given the synthetic ease of the formation of the precursors and clusters, the use of simple hydrides as initiators of cluster growth, and the high yields of the resultant nanoclusters, we set out to further explore the potential of such facile procedures for the preparation of carbonyl-ligand-free transition-metal nanoclusters with new topologies. Herein, we report the synthesis of a low-valent manganese nanosheet with a hitherto unknown arrangement of six Mn atoms in a nearly planar ladder-type architecture (**C**). Magnetic susceptibility measurements support the notion of strong antiferromagnetic interactions between the Mn ions, which result in a diamagnetic ground state. The Mn_6 cluster was

[*] Dr. U. Chakraborty, E. Reyes-Rodriguez, Prof. Dr. A. Jacobi von Wangelin
Department of Chemistry
University of Regensburg (Germany)
Dr. U. Chakraborty, Prof. Dr. A. Jacobi von Wangelin
Department of Chemistry
University of Hamburg
Martin Luther King Pl. 6, 20146 Hamburg (Germany)
E-mail: axel.jacobi@chemie.uni-hamburg.de
Dr. S. Demeshko, Prof. Dr. F. Meyer
University of Göttingen
Institute of Inorganic Chemistry
Tammannstraße 4, 37077 Göttingen (Germany)
Supporting information and the ORCID identification number(s) for the author(s) of this article can be found under: https://doi.org/10.1002/anie.201800079.

shown to be a molecular precursor to catalytically active nanoparticles, which displayed activities that are distinct from those of previously reported molecular Mn catalysts.

Substitution of the bulky amides in $M[N(SiMe_3)_2]_2$ complexes (M = Fe, Co) with hydrides has recently enabled the preparation of soluble Fe and Co nanoclusters.[3] We surmised that an equimolar reaction of the related manganese complex $Mn[N(SiMe_3)_2]_2$ (**1**)[6] with a hydride reagent would afford the coordinatively highly unsaturated species $[Mn\{N(SiMe_3)_2\}H]$. Oligomerization of this intermediate to higher aggregates constitutes a new entry into the nanoscale regime of Mn cluster growth and, in comparison with the related Fe and Co structures, provides new insight into the control of cluster topology by the nature of the 3d transition metal.

Paralleling our work with Fe and Co clusters, we were mostly interested in the identification of small soluble nanoclusters that constitute snapshots on the nanoscale of the growth of nanoparticles from low-valent molecular Mn complexes. Indeed, the reaction of **1** with 1 equiv HBpin (or Dibal-H) in *n*-hexane at 20 °C readily afforded the novel Mn_6 cluster $[Mn_6(\mu_3\text{-}H)_4(\mu_2\text{-}H)_2\{(\mu_2\text{-}N(SiMe_3)_2\}_4\{N(SiMe_3)_2\}_2]$ as brown single crystals in 18% yield after recrystallization (**2**; Scheme 1). Single-crystal X-ray analysis of **2** revealed an unprecedented ladder-type Mn_6 nanocluster containing four μ_2-bridging $N(SiMe_3)_2$ and two terminal $N(SiMe_3)_2$ ligands (Scheme 1, middle). The Mn_6 core is best described as a "flat chair" with four coplanar Mn centers (Mn_2, Mn_3, $Mn_{2'}$, and $Mn_{3'}$). Two Mn centers (Mn_1 and $Mn_{1'}$) cap two opposite edges of the central Mn_4 motif slightly above and below the plane (11.9°; see Scheme 1, right). Alternatively, this novel near-planar hexametallic architecture can be viewed as an array of four Mn_3 triangles sharing three common edges in a zigzag chain. This structural interpretation could also suggest that the stepwise growth of the Mn_6 nanocluster proceeds through sequential formal [1+2] additions of Mn_1 units across Mn–Mn bonds. The resultant M_3 triangles are the common topological motif of all members of the $(hmds)_xM_yH_z$ family (hmds = $N(SiMe_3)_2$) with Mn_6, Fe_4, Fe_6, Fe_7, and Co_7 cores.[3] The unprecedented planar growth might be a direct consequence of the steric bulk of the hmds ligands, which effectively shield the half spaces above and below the metal plane. The Mn–Mn bond lengths (2.85622(3)–2.97627(3) Å) are in the range of Mn–Mn bonds in other Mn clusters.[7,11] The positions of the hydride ligands of **2** were determined from the electron density Fourier map. Four μ_3-H atoms coordinate the Mn_6 core in alternating up and down fashion. Two μ_2-H atoms span the sterically more hindered peripheral Mn–Mn bonds whereas the least hindered peripheral Mn–Mn edges are coordinated by the bulky hmds ligands.

In an effort to elucidate key properties of **2**, we further characterized the single crystals. In C_6D_6 solution, **2** is paramagnetic and ^{1}H-NMR silent. Solid **2** is thermally highly stable; decomposition was observed at 139 °C. The UV/Vis spectrum in *n*-hexane showed a featureless broad band tailing into the visible region (see the Supporting Information, Figure S1). No significant absorption of the Mn–H moiety was detected in the expected region between 1500 and 2000 nm (Figure S2). An effective magnetic moment μ_{eff} of 4.28 μ_B (or 2.29 cm^3mol^{-1} K, per Mn_6 cluster, in C_6D_6) was recorded, which is much lower than the spin-only value for six uncoupled $S = 5/2$ spins (14.49 μ_B or 26.25 cm^3mol^{-1}K). This may indicate the presence of strong antiferromagnetic interactions. Thus the temperature-dependent magnetism was analyzed by a SQUID measurement on solid **2** ($\chi_M T$ vs. T plot in Figure 2). Indeed, $\chi_M T$ drops rapidly and approaches zero at low temperatures, which supports the assumption of strong antiferromagnetic exchange and a diamagnetic ground state. Coupling constants were obtained

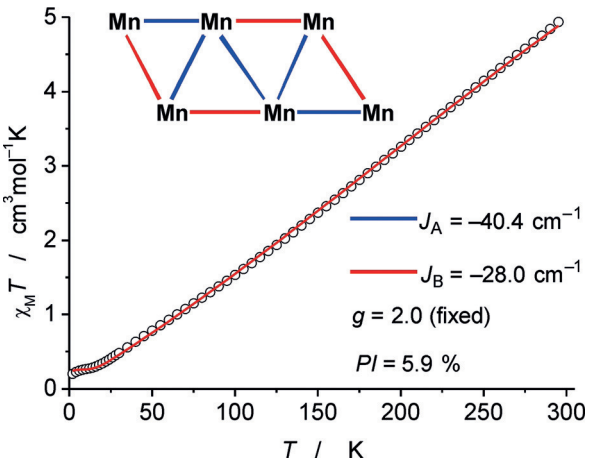

Figure 2. Temperature dependence of $\chi_M T$ for **2**. The solid red line is the best fit. See the main text and the Supporting Information for details. Inset: magnetic coupling pattern used for the simulation.

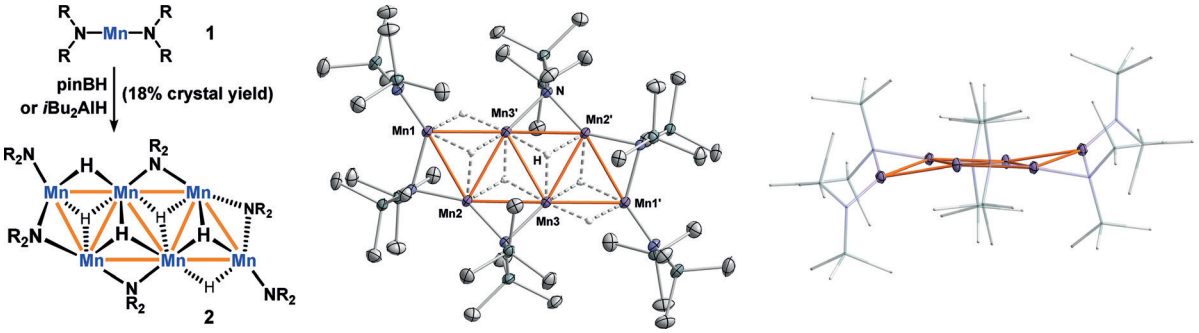

Scheme 1. Synthesis of the Mn_6 cluster **2** (left). Center and right: Crystal structure of **2**. Ellipsoids set at 50% probability. Hydrogen atoms omitted except for Mn–H.

from fitting the data on the basis of a simplified spin Hamiltonian that includes two coupling constants and Zeeman splitting, using the PHI program.[8] The coupling pattern shown in the inset in Figure 2 was derived from the structural data, where red lines represent coupling through amide and hydride ligands, and blue lines represent couplings only through hydride ligands. To avoid over-parametrization, the *g* values for all Mn ions were fixed to 2.0. The obtained coupling constants $J_A = -40.4\ cm^{-1}$ and $J_B = -28.0\ cm^{-1}$ lie in the same range as for trinuclear Mn_3 clusters with comparable Mn–Mn distances.[11e]

To date, all oligonuclear clusters with more than five Mn atoms reported in the literature contained carbonyl and multidentate N,O-ligands and adopted three-dimensional polyhedral geometries.[7,9,10] Two-dimensional Mn clusters are very rare;[11] no carbonyl-free 2D hexametal skeleton has ever been reported. Two planar Mn_7 wheels of type **A** (Figure 1) are contained within $[Mn][Mn_7(THF)_6(CO)_{12}]_2$, where each $Mn_7(THF)_6(CO)_{12}^-$ anion is coordinated to an isolated Mn^{2+} cation via three carbonyl oxygen atoms to give an octahedral coordination geometry about the central cation.[4c] A ladder-type hexametallic skeleton was observed in the complex $[Os_6(CO)_{18}(O_2CCF_3)]$.[5] The isolation of the Mn_6 cluster **2** presents tangible advances over the current state of the art of nanocluster topologies: **2** adopts a rare flat-chair geometry of six metal centers, it is free of strongly coordinating CO ligands, but contains labile amide and hydride ligands, the linear zigzag cluster growth is distinct from that of the recently reported Fe and Co clusters, and the manganese ions show strong antiferromagnetic interactions. Generally, discrete metal clusters receive great interest owing to their special optical, magnetic, and catalytic properties.[12] This first report of an easily accessible, soluble, planar oligo(hydridomanganese) nanosheet is of direct relevance for the design and understanding of hydrogen storage materials and hydrogenation catalysts.[3,13]

An initial survey of the general reactivity pattern of **2** towards various reagents is shown in Scheme 2. The reaction of **2** with 10 equiv benzaldehyde gave benzyl alcohol (55% vs. benzaldehyde), which indicates the presence of more than five active hydride ligands in **2**. The hydride reactivity was insufficient towards the poor electrophiles 4-bromoanisol (no debromination), diphenylacetylene (ca. 1% stilbene per Mn), and 1-octene. Upon addition of 4-methylpyridine (^{Me}Py, 6 equiv), a yellow solution of **2** in C_6D_6 afforded a brown solution of a paramagnetic compound exhibiting broad ^{1}H NMR resonances but no free ^{Me}Py. Further addition of ^{Me}Py (12 equiv) shifted the broad ^{1}H NMR resonances towards those of free ^{Me}Py, presumably owing to an equilibrium between coordinated and free ^{Me}Py. Addition of 1 equiv Dibal-H or pinBH to **2** resulted in a black solution, presumably owing to degradation of the complex to soluble Mn nanoparticles (see below). The first Mn-catalyzed cyclotrimerization of alkynes was observed. Phenylacetylene was converted into triphenylbenzene isomers (up to 50% yield) in the presence of 0.83 mol% **2**.[14] Sequential treatment of **2** (1.66 mol%) with ^{Me}Py and pinacolborane (HBpin) gave no hydroboration product, whereas the reverse order of addition (**2**, HBpin, ^{Me}Py) enabled selective 1,2-hydroboration (74% yield).[15] The in situ prepared cluster **2** (from $Mn(hmds)_2$ and HBpin) exhibited similar hydroboration activity. As hydride transfer appeared to be especially favorable with **2**, we turned our attention to the investigation of hydrogenations in the presence of catalytic amounts of **2**.

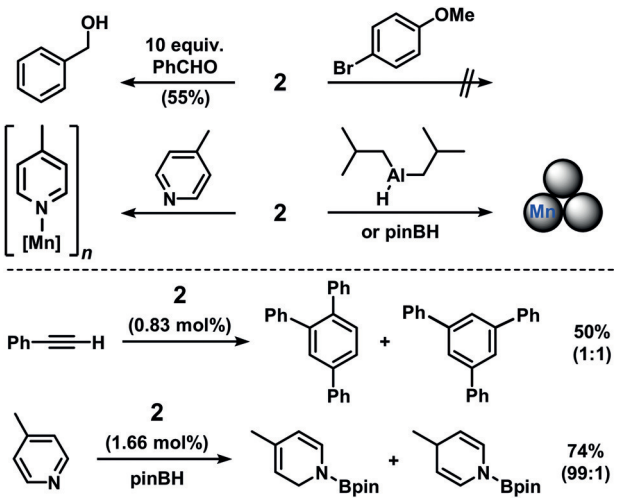

Scheme 2. Survey of stoichiometric (top) and catalytic (bottom) reactions of **2**.

Hydrogenations of C=C and C=X bonds have mostly been performed with noble-metal catalysts.[16] The use of inexpensive, abundant, and non-toxic base metals has only recently been evaluated in the context of hydrogenations.[17] Manganese, as an early 3d transition metal, has largely been neglected in the development of potential hydrogenation catalysts, despite its high natural abundance (3rd most abundant transition metal in the Earth's crust after Fe, Ti) and biocompatibility.[18] In the past three years, only a handful of homogeneous pincer-type Mn complexes were applied to hydrogenations of polar C=X bonds, such as carbonyl and nitrile compounds as well as carbon dioxide, by the groups of Beller,[19] Kempe,[20] Milstein,[21] and others.[22] On the other hand, Mn-catalyzed hydrogenations of less polar C=X and non-polar C=C bonds have not been significantly explored.[18] There are two very early examples of the hydrogenation and isomerization of octenes with $Mn_2(CO)_{10}$ under harsh thermal conditions (207 bar H_2, 160 °C)[23] or with *cis*-$[(CO)_4(PPh_3)MnH]$ under UV light irradiation.[24] The trinuclear carbonyl cluster $[\{Mn(CO)_3\}_3H_3]$[25] was shown to coordinate alkenes and alkynes;[26] however, no further transformations were studied. To the best of our knowledge, there is no report on efficient Mn-catalyzed hydrogenations of less polar unsaturated substrates, such as alkenes, alkynes, or imines.

We investigated the hydrogenation of α-methylstyrene (**3**) and 1-phenyl-1-cyclohexene (**4**) under mild conditions (Table 1). Mn_6 cluster **2** (0.83 mol% = 5 mol% Mn) was inactive at 2 bar H_2 and 20 °C, but catalyzed full conversion of **3** at 5 bar H_2 and 60 °C. However, the latter conditions led to catalyst precipitation (in *n*-heptane) or a rapid color change from yellow to dark brown (in C_6D_6). Very good catalyst activity at 2 bar H_2 and 20 °C was observed when employing equimolar amounts of Dibal-H and **2** (entry 3). The same activity was achieved by in situ formation of **2** (from 5 mol%

Table 1: Optimization of the manganese-catalyzed alkene hydrogenation.

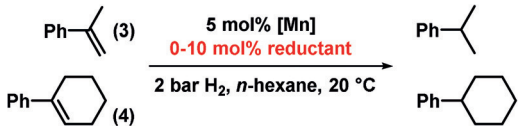

Entry	Catalyst	Reductant (mol%)	Ph-*i*Pr [%]	Ph-Cy [%]
1	**2**	–	0	
2[a]	**2**	–	100	
3	**2**	iBu_2AlH (5)	97	
4[b]	$Mn(hmds)_2$	iBu_2AlH (10)	97	
5	$Mn(hmds)_2$	pinBH (5 or 10)		0
6	$Mn(hmds)_2$	iBu_2AlH (5)		0
7	**$Mn(hmds)_2$**	**iBu_2AlH (10)**		**>99**
8	$Mn(hmds)_2$	–		0
9[c]	$MnBr_2$	iBu_2AlH (10)		0
10[d]	$Mn(hmds)_2$	iBu_2AlH (10)		2

General reactions conditions: alkene (0.2 mmol), [Mn] (5 mol%), reductant, hexane (1 mL), 2 bar H_2 (for **3**), 5 bar H_2 (for **4**), 20°C, 20 h. [a] 5 bar H_2, 60°C. [b] In situ formation of **2** from $Mn(hmds)_2$ and Dibal-H prior to addition of another 5 mol% Dibal-H. [c] $MnBr_2$ (5 mol%) in THF. [d] $MnBr_2$ (5 mol%), $LiN(SiMe_3)_2$ (10 mol%) in toluene instead of $Mn(hmds)_2$. Yields determined by quantitative GC-FID analysis with *n*-pentadecane as an internal standard.

$Mn(hmds)_2$/Dibal-H in *n*-hexane) followed by addition of another 5 mol% of Dibal-H (entry 4). Further optimization with the more challenging trisubstituted substrate 1-phenyl-1-cyclohexene (**4**) was in full agreement with the fact that the binary catalyst system $Mn(hmds)_2$/Dibal-H (1:2) was the most active hydrogenation catalyst in a non-polar solvent such as *n*-hexane (entry 7). Pinacolborane effected the formation of **2** (Scheme 1), but gave an inactive catalyst when mixed with $Mn(hmds)_2$ under the reaction conditions (entries 5 and 6). The optimized reaction conditions were applied to hydrogenate various alkenes (Table 2).

Mono- and disubstituted alkenes were hydrogenated at 5 bar H_2 and room temperature in high yields. Turnover frequencies of 65 and 24 h^{-1} were observed for the hydrogenation of 1-octene and α-methylstyrene, respectively, at 2 bar H_2 and 20°C after 5 min. The mild reaction conditions tolerated fluoride, thioether, ether, amine, and benzyl substituents. Trisubstituted alkenes were quantitatively converted at 10 bar H_2 and 60°C (entries 19–24). Alkynes underwent clean hydrogenation to the alkanes (entries 26–28). A few key mechanistic experiments were performed: No adduct was obtained for the hydrogenation of **3** in the presence of the radical trap triphenylethylene. The catalyst activity was quenched in the presence of ethyl 3,3-dimethylacrylate. Employment of the radical clock α-cyclopropyl styrene generated a small amount of the ring-opened product (9%), but mainly the hydrogenation product (91%).[27] A competition experiment with 4-methoxy-α-methylstyrene and 4-trifluoromethyl-α-methylstyrene showed that the electron-rich alkene is hydrogenated more than three times faster (Scheme 3), which could be explained by the stronger coordination of the more Lewis basic substrate to the catalyst (see also Scheme 2). Following this observation, we extended the scope of the Mn-catalyzed hydrogenation to imines, which

Table 2: Manganese-catalyzed alkene hydrogenation.

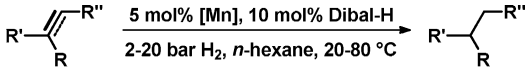

Entry	Alkene	Substituents	Yield [%]
1	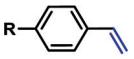	R = H	81
2		R = F	80
3		R = Ph	75
4[a]		R = *n*-C_5H_{11}	72 (94)
5		R = Me	100
6		R = *n*-Pr	94
7		R = cyclopropyl	91
8		R = Ph	84
9[b]	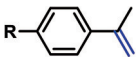	R = F	81 (81)
10[c]		R = Cl	8 (15)
11		R = Br	0 (0)
12		R = SMe	25 (38)
13		R = OMe	99
14		R = Me	96
15			100
16[d]	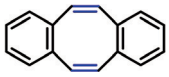		56 (70)
17			76
18	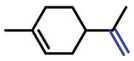		73[e]
19[f]		R = Me	100
20[f]		R = Ph	94 (94)
21		*n* = 1	100
22		*n* = 2	>99
23		*n* = 3	45 (47)
24	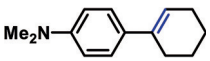		94 (94)
25[g]	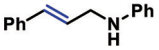		89[e]
26		$R^1 = R^2$ = Ph	96
27		R^1 = Ph, R^2 = Me	77
28		$R^1 = R^2$ = *n*-C_5H_{11}	87

Standard reaction conditions: alkene or alkyne (0.2 mmol), Mn[N-$(SiMe_3)_2]_2$ (5 mol%), Dibal-H (10 mol%), *n*-hexane, 20°C; 2 bar H_2, 3 h (entries 1–5); 5 bar H_2, 20 h (entries 6–28). If not otherwise noted, yields were determined by quantitative GC-FID analysis with *n*-pentadecane as an internal standard; conversions given in parentheses if not >95%. [a] Traces of isomerization. [b] 5 bar H_2, 3 h. [c] α-Methylstyrene (1%) formed. [d] Mixture of dihydro and tetrahydro products (4:1). [e] Yield of isolated product. [f] 10 bar H_2, *n*-heptane, 60°C. [g] 20 bar H_2, *n*-heptane, 80°C.

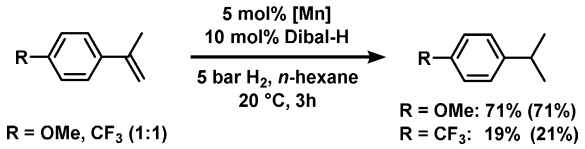

Scheme 3. Competitive hydrogenation of electron-rich versus electron-poor alkenes.

have not been studied in the literature. Very good conversions were achieved with *N*-aryl and *N*-alkyl aldimines (Table 3). Conjugated styrenyl aldimines underwent highly chemoselective C=N hydrogenation (entries 6–9), which suggests catalyst poisoning by the resulting amine. The higher reactivity of 8-methylquinoline versus quinoline might also be a direct consequence of unproductive σ-coordination of the latter to the catalyst (entries 11 and 12; see Scheme 1).

The clear distinction between homogeneous and heterogeneous catalysis mechanisms is not trivial. However, kinetic studies are an instructive tool to discriminate between monometal and cluster catalysts by the analysis of selective poisoning experiments.[28] Addition of "sub-catalytic" amounts of trimethylphosphine at about 30% conversion of α-methylstyrene led to complete catalyst inhibition already at a catalyst/poison ratio of 5:1 (Scheme S1).[28] Hydrogenation of α-cyclopropyl styrene was only slightly slower in the presence of the homotopic poison dibenzo-[*a*,*e*]cyclooctatetraene[29] (dct, 4 equiv per Mn), which acted as a competing substrate (see the Supporting Information and Table 2, entry 16). These results are strong indications of a heterotopic reaction mechanism involving polynuclear low-valent Mn species that are formed upon reductive activation of the nanocluster **2** with hydride reagents.

In summary, we have reported an unprecedented ladder-type $[XMnH]_6$ cluster that contains bulky amido ligands and active hydrides. This nanosheet complements the small family of planar 3d transition-metal clusters and presents a novel cluster topology. The cluster is soluble in organic solvents; its crystals were studied by X-ray crystallography and solid-state SQUID measurements. The latter evidences strong antiferromagnetic exchange interactions and a diamagnetic ground state for **2**. Under reducing conditions, the nanocluster displayed unprecedented catalytic activity in hydrogenations of alkenes, alkynes, and imines. Extensions of such nanocluster preparations and applications in small-molecule activation are currently being explored.

Table 3: Manganese-catalyzed imine hydrogenation.

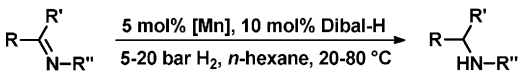

Entry	Imine	Substituents	Yield [%]
1	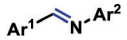	$Ar^1 = Ar^2 = Ph$	93
2		Ar^1 = 4-$MeOC_6H_4$, $Ar^2 = Ph$	96
3[a]		$Ar^1 = Ph$, Ar^2 = 4-$MeSC_6H_4$	93
4	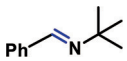		89
5	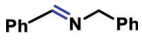		50[b] (57)
6[a]	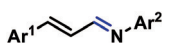	$Ar^1 = Ar^2 = Ph$	96
7[a,c]		Ar^1 = 4-$MeOC_6H_4$, $Ar^2 = Ph$	89[d]
8[a,c]		Ar^1 = 4-FC_6H_4, $Ar^2 = Ph$	83[d]
9[a,c]		Ar^1 = 4-$Me_2NC_6H_4$, $Ar^2 = Ph$	74[d]
10[a]	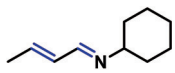		54
11[a]	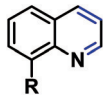	R = H	11[b] (18)
12[a]		R = Me	55
13[a]	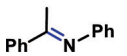		93

Standard reaction conditions: imine (0.2–0.5 mmol), $Mn[N(SiMe_3)_2]_2$ (5 mol%), Dibal-H (10 mol%), *n*-hexane, 5 bar H_2, 20°C. If not otherwise noted, yields of isolated products are given. [a] 20 bar H_2, *n*-heptane, 80°C, 20 h; [b] Yield determined by quantitative GC-FID with *n*-pentadecane as an internal standard; conversions in parentheses if not >95%. [c] Ca. 10% alkene hydrogenation. [d] Yield determined by ^{1}H NMR spectroscopy.

Acknowledgements

This work was funded by the European Research Council (ERC) through a Consolidator grant (683150). S.D. and F.M. acknowledge support from the University of Göttingen.

Conflict of interest

The authors declare no conflict of interest.

Keywords: clusters · hydrides · hydrogenation · manganese · nanosheets

How to cite: *Angew. Chem. Int. Ed.* **2018**, *57*, 4970–4975
Angew. Chem. **2018**, *130*, 5064–5069

[1] a) A. J. Mannix, B. Kiraly, M. C. Hersam, N. P. Guisinger, *Nat. Rev. Chem.* **2017**, *1*, 0014; b) A. K. Geim, I. V. Grigorieva, *Nature* **2013**, *499*, 419; c) A. K. Geim, K. S. Novoselov, *Nat. Mater.* **2007**, *6*, 183.
[2] M. Osada, T. Sasaki, *Adv. Mater.* **2012**, *24*, 210.
[3] For carbonyl-free 2D metal clusters, see: a) T. N. Gieshoff, U. Chakraborty, M. Villa, A. Jacobi von Wangelin, *Angew. Chem. Int. Ed.* **2017**, *56*, 3585; *Angew. Chem.* **2017**, *129*, 3639; b) R. Araake, K. Sakadani, M. Tada, Y. Sakai, Y. Ohki, *J. Am. Chem. Soc.* **2017**, *139*, 5596; c) Y. Ohki, Y. Shimizu, R. Araake, M. Tada, W. M. C. Sameera, J.-I. Ito, H. Nishiyama, *Angew. Chem. Int. Ed.* **2016**, *55*, 15821; *Angew. Chem.* **2016**, *128*, 16053; d) S. K. Brayshaw, J. C. Green, R. Edge, E. J. L. McInnes, P. R. Raithby, J. E. Warren, A. S. Weller, *Angew. Chem. Int. Ed.* **2007**, *46*, 7844; *Angew. Chem.* **2007**, *119*, 7990; e) E. Cerrada, M. Contel, A. D. Valencia, M. Laguna, T. Gelbrich, M. B. Hursthouse, *Angew. Chem. Int. Ed.* **2000**, *39*, 2353; *Angew. Chem.* **2000**, *112*, 2443.
[4] For 2D metal–CO clusters, see: a) R. D. Adams, Q. Zhang, X. Yang, *J. Am. Chem. Soc.* **2011**, *133*, 15950, and references therein; b) S. Du, B. E. Hodson, P. Lei, T. D. McGrath, F. G. A. Stone, *Inorg. Chem.* **2007**, *46*, 6613; c) G. Kong, G. N. Harakas,

B. R. Whittlesey, *J. Am. Chem. Soc.* **1995**, *117*, 3502; d) M. P. Diebold, S. R. Drake, B. F. G. Johnson, J. Lewis, M. McPartlin, H. Powell, *J. Chem. Soc. Chem. Commun.* **1988**, *0*, 1358; e) G. Doyle, K. A. Eriksen, D. Van Engen, *J. Am. Chem. Soc.* **1986**, *108*, 445.

[5] S. Zacchini, *Eur. J. Inorg. Chem.* **2011**, 4125, and references therein.

[6] P. P. Power, *Chem. Rev.* **2012**, *112*, 3482.

[7] a) C. E. Holloway, M. Melnik, *J. Organomet. Chem.* **1990**, *396*, 129; b) D. M. P. Mingos, A. S. May in *The Chemistry of Metal Cluster Complexes* (Eds.: D. F. Shriver, H. D. Kaesz, R. D. Adams), VCH, New York, **1990**, p. 11.

[8] N. F. Chilton, R. P. Anderson, L. D. Turner, A. Soncini, K. S. Murray, *J. Comput. Chem.* **2013**, *34*, 1164.

[9] A. R. Fout, Q. Zhao, D. J. Xiao, T. A. Betley, *J. Am. Chem. Soc.* **2011**, *133*, 16750.

[10] H. J. Eppley, H.-L. Tsai, N. de Vries, K. Folting, G. Christou, D. N. Hendrickson, *J. Am. Chem. Soc.* **1995**, *117*, 301.

[11] For examples of Mn_3 clusters, see: a) E. W. Abel, I. D. H. Towle, T. S. Cameron, R. E. Cordes, *J. Chem. Soc. Dalton Trans.* **1979**, 1943; b) P. Legzdins, C. R. Nurse, S. J. Rettig, *J. Am. Chem. Soc.* **1983**, *105*, 3727; c) Z. G. Fang, T. S. A. Hor, K. F. Mok, S. C. Ng, L. K. Liu, Y. S. Wen, *Organometallics* **1993**, *12*, 1009; d) K.-C. Huang, Y.-C. Tsai, G.-H. Lee, S.-M. Peng, M. Shieh, *Inorg. Chem.* **1997**, *36*, 4421; e) A. R. Fout, D. J. Xiao, Q. Zhao, T. D. Harris, E. R. King, E. V. Eames, S.-L. Zheng, T. A. Betley, *Inorg. Chem.* **2012**, *51*, 10290.

[12] a) *Metal Clusters in Catalysis* (Eds.: B. C. Gates, L. Guczi, H. Knözinger), Elsevier, Amsterdam, **1986**; b) H. H. Lamb, B. C. Gates, H. Knözinger, *Angew. Chem. Int. Ed. Engl.* **1988**, *27*, 1127; *Angew. Chem.* **1988**, *100*, 1162; c) *Metal Clusters in Chemistry* (Eds.: P. Braunstein, L. A. Oro, P. R. Raithby), Wiley-VCH, Weinheim, **1999**; d) E. de Smit, B. M. Weckhuysen, *Chem. Soc. Rev.* **2008**, *37*, 2758; for magnetic applications, see: e) R. Sessoli, D. Gatteschi, A. Caneschi, M. A. Novak, *Nature* **1993**, *365*, 141; f) R. Sessoli, H. L. Tsai, A. R. Schake, S. Wang, J. B. Vincent, K. Folting, D. Gatteschi, G. Christou, D. N. Hendrickson, *J. Am. Chem. Soc.* **1993**, *115*, 1804; g) D. Gatteschi, R. Sessoli, J. Villain, *Molecular Nanomagnets*, Oxford University Press, Oxford, **2006**; h) G. Karotsis, S. J. Teat, W. Wernsdorfer, S. Piligkos, S. J. Dalgarno, E. K. Brechin, *Angew. Chem. Int. Ed.* **2009**, *48*, 8285; *Angew. Chem.* **2009**, *121*, 8435.

[13] a) T. Shima, Y. Luo, T. Stewart, R. Bau, G. J. McIntyre, S. A. Mason, Z. Hou, *Nat. Chem.* **2011**, *3*, 814; b) R. D. Adams, B. Captain, *Angew. Chem. Int. Ed.* **2008**, *47*, 252; *Angew. Chem.* **2008**, *120*, 258; c) A. S. Weller, J. S. McIndoe, *Eur. J. Inorg. Chem.* **2007**, 4411; d) J. M. Thomas, R. Raja, B. F. G. Johnson, S. Hermans, M. D. Jones, T. Khimyak, *Ind. Eng. Chem. Res.* **2003**, *42*, 1563.

[14] D. Brenna, M. Villa, T. N. Gieshoff, F. Fischer, M. Hapke, A. Jacobi von Wangelin, *Angew. Chem. Int. Ed.* **2017**, *56*, 8451; *Angew. Chem.* **2017**, *129*, 8571.

[15] S. Park, S. Chang, *Angew. Chem. Int. Ed.* **2017**, *56*, 7720; *Angew. Chem.* **2017**, *129*, 7828.

[16] a) *The Handbook of Homogeneous Hydrogenation* (Eds.: J. G. de Vries, C. J. Elsevier), Wiley-VCH, Weinheim, **2007**; b) S. Nishimura, *Handbook of Heterogeneous Catalytic Hydrogenation for Organic Synthesis*; Wiley, New York, **2001**.

[17] a) *Catalysis without Precious Metals* (Ed.: R. M. Bullock), Wiley-VCH, Weinheim, **2010**; b) P. J. Chirik, *Acc. Chem. Res.* **2015**, *48*, 1687; c) K. Junge, K. Schröder, M. Beller, *Chem. Commun.* **2011**, *47*, 4849; d) B. A. F. Le Bailly, S. P. Thomas, *RSC Adv.* **2011**, *1*, 1435.

[18] D. A. Valyaev, G. Lavigne, N. Lugan, *Coord. Chem. Rev.* **2016**, *308*, 191.

[19] a) S. Elangovan, C. Topf, S. Fischer, H. Jiao, A. Spannenberg, W. Baumann, R. Ludwig, K. Junge, M. Beller, *J. Am. Chem. Soc.* **2016**, *138*, 8809; b) S. Elangovan, M. Garbe, H. Jiao, A. Spannenberg, K. Junge, M. Beller, *Angew. Chem. Int. Ed.* **2016**, *55*, 15364; *Angew. Chem.* **2016**, *128*, 15590; c) M. Perez, S. Elangovan, A. Spannenberg, K. Junge, M. Beller, *ChemSusChem* **2017**, *10*, 83.

[20] F. Kallmeier, T. Irrgang, T. Dietel, R. Kempe, *Angew. Chem. Int. Ed.* **2016**, *55*, 11806; *Angew. Chem.* **2016**, *128*, 11984.

[21] N. A. Espinosa-Jalapa, A. Nerush, L. J. W. Shimon, G. Leitus, L. Avram, Y. Ben-David, D. Milstein, *Chem. Eur. J.* **2017**, *23*, 5934.

[22] a) R. van Putten, E. A. Uslamin, M. Garbe, C. Liu, A. Gonzalez-de-Castro, M. Lutz, K. Junge, E. J. M. Hensen, M. Beller, L. Lefort, E. A. Pidko, *Angew. Chem. Int. Ed.* **2017**, *56*, 7531; *Angew. Chem.* **2017**, *129*, 7639; b) A. Dubey, L. Nencini, R. R. Fayzullin, C. Nervi, J. R. Khusnutdinova, *ACS Catal.* **2017**, *7*, 3864; c) F. Kallmeier, R. Kempe, *Angew. Chem. Int. Ed.* **2018**, *57*, 46.

[23] T. A. Weil, S. Metlin, I. Wender, *J. Organomet. Chem.* **1973**, *49*, 227.

[24] P. L. Bogdan, P. J. Sullivan, T. A. Donovan, J. D. Atwood, *J. Organomet. Chem.* **1984**, *269*, c51.

[25] S. W. Kirtley, J. P. Olsen, R. Bau, *J. Am. Chem. Soc.* **1973**, *95*, 4532, and references therein.

[26] R. B. King, M. N. Ackermann, *Inorg. Chem.* **1974**, *13*, 637.

[27] a) R. M. Bullock, E. G. Samsel, *J. Am. Chem. Soc.* **1990**, *112*, 6886; b) J. Masnovi, E. G. Samsel, R. M. Bullock, *J. Chem. Soc. Chem. Commun.* **1989**, 1044.

[28] R. H. Crabtree, *Chem. Rev.* **2012**, *112*, 1536.

[29] a) D. R. Anton, R. H. Crabtree, *Organometallics* **1983**, *2*, 855; b) G. Franck, M. Brill, G. Helmchen, *J. Org. Chem.* **2012**, *89*, 55.

Manuscript received: January 3, 2018
Revised manuscript received: February 5, 2018
Accepted manuscript online: February 13, 2018
Version of record online: March 22, 2018

